Pergamon

J. Mech. Phys. Solids, Vol. 42, No. 11, pp. 1743–1766, 1994

0022–5096/94 $7.00 + 0.00

0022–5096(94)00044–1

MICROBUCKLING OF FIBER COMPOSITES WITH RANDOM INITIAL FIBER WAVINESS

W. S. SLAUGHTER† and N. A. FLECK‡

†University of Pittsburgh, Mechanical Engineering Department, Pittsburgh, PA 15261, U.S.A. and
‡Cambridge University Engineering Department, Cambridge CB2 1PZ, U.K.

(*Received* 20 *January* 1994; *in revised form* 22 *June* 1994)

ABSTRACT

A fiber microbuckling calculation is presented for the effects of fiber misalignment and material nonlinearity on the compressive strength of fiber composites. The role of fiber bending stiffness is included by using a particular form of couple stress theory. In order to examine the effect of a distribution of fiber waviness, the fiber misalignment angle is assumed to vary along the fiber length but is taken to be uniform in the transverse direction. Thus, the effects of wavelength as well as amplitude of fiber waviness are taken into account. A consideration of sinusoidal initial waviness reveals that short wavelength imperfections are much less deleterious than long wavelengths. A statistical analysis is presented for the effect of random fiber waviness on compressive strength, using a Monte Carlo simulation technique. Compressive strength is found to be particularly sensitive to the area under the spectral density curve and to the minimum fiber wavelength.

INTRODUCTION

Modern engineering fiber composites are increasingly used in applications where their high specific tensile moduli and specific tensile strengths outweigh competing cost considerations. This is particularly evident in the aerospace, automotive and sporting goods industries. However, the *compressive* strengths of long, aligned fiber composites may be as low as 60% of their tensile strength and the compressive strength is recognized to be a design limiting consideration. An understanding of the phenomena involved in compressive failure is crucial to the development of improved composite materials.

It has been shown that the critical mechanism in the compressive failure of polymer matrix composites is plastic microbuckling (Argon, 1972; Budiansky and Fleck, 1993). Microbuckling is the failure mechanism by which the composite suffers localized collapse within a kink band (Hull, 1981; Daniel *et al.*, 1993). The kink band is typically of the order of 10 fiber diameters in width and the normal to the kink band is at an angle $\beta = 15$–30° to the fiber direction. The role of microbuckling in the compressive failure of metal matrix and ceramic matrix composites is less clear, although it has been observed in aluminum alloy composites (Schulte and Minoshima, 1991) and in carbon–carbon composites (Evans and Adler, 1978). Microbuckling may also play an important role in compression–compression fatigue (Huang and Wang,

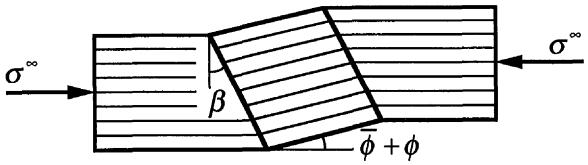

Fig. 1. Sketch of a microbuckle band used in the kinking model.

1989; Slaughter and Fleck, 1993a) and in the compressive creep failure of aligned fiber composites (Jelf, 1993; Schapery, 1993; Slaughter and Fleck, 1993b; Slaughter *et al.*, 1993).

Several micromechanical models have been developed which attempt to predict the critical stress for microbuckling of aligned fiber composites. Rosen (1965) modeled microbuckling as an elastic bifurcation phenomenon. For sufficiently large fiber volume concentrations, the Rosen model predicts a critical stress for microbuckling given by

$$\sigma_c^\infty = G, \tag{1}$$

where σ_c^∞ is the critical remote compressive stress parallel to the fiber axes and G is the composite in-plane shear modulus. If the shear modulus for the fibers is large compared to the shear modulus of the matrix G_m, then

$$G = G_m/(1-c), \tag{2}$$

where c is the fiber volume concentration. A comparison with experimental results shows that (1) overestimates the critical stress for microbuckling by a factor of about four.

Several investigators have examined models of microbuckling which improve upon some of the approximations made by Rosen (1965), but continue to treat microbuckling as an elastic bifurcation event. Sadowsky *et al.* (1967) have constructed a three-dimensional model of microbuckling and Steif (1987) has taken into account finite strains and material nonlinearity in both constituents of a fiber composite. Lagoudas *et al.* (1991) have considered the stability of small perturbations in fiber displacement, with variable characteristic wavelength, superimposed upon a uniform applied compressive strain. Christensen (1993) has examined the competition between fiber composite material instability, in the form of an elastic bifurcation, and structural instability of a composite shell structure as a whole. These and other analyses based on elastic bifurcation all overestimate the critical stress for microbuckling.

An alternative approach based on a model of microbuckling as a plastic collapse event was first proposed by Argon (1972). In this model the fibers are misaligned by an angle $\bar{\phi}$, within a band, as shown in Fig. 1. In Argon's analysis this band is taken to be normal to the fiber direction ($\beta = 0$). The fibers are assumed to be inextensible and suffer a remote compressive axial stress; the associated deformation within the kink band is given by the additional rotation ϕ of the fibers. For a rigid–perfectly plastic composite response, the critical stress for microbuckling is given by

$$\sigma_c^\infty = \frac{\tau_y}{\bar{\phi}}, \tag{3}$$

where τ_y is the plane strain yield stress of the composite in pure shear. Budiansky (1983) extended this result for an elastic–perfectly plastic composite response and found

$$\sigma_c^\infty = \frac{\tau_y}{\gamma_y + \bar{\phi}} = \frac{G}{1 + \bar{\phi}/\gamma_y}, \tag{4}$$

where $\gamma_y \equiv \tau_y/G$ is the in-plane shear yield strain of the composite. This result reduces to the Rosen bifurcation solution (1) when $\bar{\phi} = 0$ and is asymptotically equivalent to Argon's result (3) in the limit $\bar{\phi}/\gamma_y \gg 1$.

Jelf and Fleck (1992) have shown that, for polymer matrix composites, experimental evidence supports the plastic collapse model of microbuckling. Budiansky and Fleck (1993) have considered the effect of nonzero kink band angle ($\beta \neq 0$), combined remote axial compression and in-plane shear loading, and plastic strain hardening on the predicted critical stress for microbuckling. [The study was extended by Slaughter *et al.* (1993) to consider general remote in-plane loading.] A Ramberg–Osgood strain hardening solid was considered, wherein the in-plane shear response is described by the three-parameter relation

$$\frac{\gamma}{\gamma_y} = \frac{\tau}{\tau_y} + \frac{3}{7}\left(\frac{\tau}{\tau_y}\right)^n. \tag{5}$$

Here, τ and γ are the in-plane shear stress and strain, respectively, of the composite and n is the hardening parameter; τ_y is interpreted as the shear yield strength and $\gamma_y \equiv \tau_y/G$ is the shear yield strain. The initial slope of the τ vs γ curve defined by (5) equals the shear modulus G. Budiansky and Fleck (1993) found that the compressive strength is given by

$$\sigma_c^\infty = \frac{\alpha^2 G}{1 + n\left(\frac{3}{7}\right)^{1/n}\left(\frac{\alpha\bar{\phi}/\gamma_y}{n-1}\right)^{(n-1)/n}}, \tag{6}$$

where $\alpha \equiv \sqrt{1 + R^2 \tan^2\beta}$, $R \equiv \sigma_{Ty}/\tau_y$ and σ_{Ty} is the plane strain yield strength of the composite in pure transverse tension. In the limit $n \to \infty$, (5) reduces to an elastic–perfectly plastic material description and, if $\beta = 0$, (6) reduces to the elastic–perfectly plastic prediction given by (4).

A different method for characterizing the nonlinear, inelastic behavior of fiber composites was employed in Schapery's (1994) analysis of plastic collapse. Schapery showed that the constitutive parameters of the composite could be expressed as functions of a single internal state variable representing the change in the microstructure. The compressive strength results are in line with those of Budiansky and Fleck (1993).

The plastic collapse models of microbuckling discussed so far assume that the fibers have zero bending stiffness, or equivalently, that they are broken at the boundaries of the kink band. As a consequence, there is no length scale associated with the fibers in the analysis. This form of model will be referred to as a *kinking model* of microbuckling. An alternative *couple stress model* which takes fiber bending stiffness

into account has been developed by Fleck *et al.* (1993). The couple stress model may be used to investigate the effect of shape of initial fiber misalignment upon critical stress. Fleck *et al.* (1993) considered an imperfection in the form of a band where the fiber misalignment angle takes the form of a half sinusoid with respect to distance along the fiber direction. In so doing, they were able to predict the kink band width. In the current paper, the critical stress for microbuckling will be predicted for two geometrical forms of fiber waviness: sinusoidal initial fiber misalignments and randomly misaligned fibers.

COUPLE STRESS MODEL

A model is presented for the compressive strength of an aligned fiber composite, including the effects of fiber bending. The development given here follows that outlined by Fleck *et al.* (1993). A remote compressive stress σ^∞ is applied along the mean fiber direction of the composite. Define a Cartesian coordinate system (x, y) with unit vectors $\mathbf{i}$ in the mean fiber direction and $\mathbf{j}$ in the transverse direction, as shown in Fig. 2. The initial fiber misalignment is defined by the initial angle $\bar{\phi}(x, y)$ between the fiber axis and the mean axial direction; subsequent fiber rotation associated with deformation of the composite is denoted by $\phi(x, y)$. Assume that the fibers are perfectly correlated along the direction $\mathbf{c} = -\sin\beta\mathbf{i} + \cos\beta\mathbf{j}$, as shown in Fig. 2. Then, $\bar{\phi}$ and ϕ can be uniquely expressed as functions of $x + y\tan\beta$ only and β is the angle a kink band forms with the fiber direction (see Fig. 1).

Kinematics

Assume that the fibers are inextensible, that $\bar{\phi}$ and ϕ are small and that the displacement $\mathbf{u} = u\mathbf{i} + v\mathbf{j}$ is constant along the correlation direction $\mathbf{c}$. The displacements are related to the fiber rotation ϕ by

$$\left.\begin{aligned} u &\approx 0 \\ \frac{\partial v}{\partial x} &\approx \phi \end{aligned}\right\}. \tag{7}$$

From (7), the axial strain in the composite is zero (to second order in ϕ) and the shear strain γ and the transverse strain ε_T are

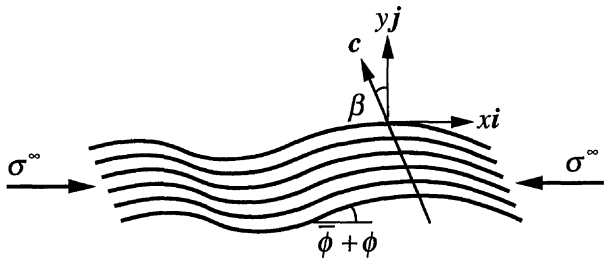

Fig. 2. Sketch of the composite fiber profile used in the couple stress model.

$$\left.\begin{aligned} \gamma &\approx \phi \\ \varepsilon_T &= \frac{\partial v}{\partial y} = \frac{\partial v}{\partial x}\tan\beta \approx \phi \tan\beta \end{aligned}\right\}. \tag{8}$$

Equilibrium

Consider the bulk composite response as illustrated by the homogeneous material element shown in Fig. 3. The composite stresses shown in Fig. 3 represent the local average of stresses in the fibers and matrix. σ_L and σ_T are the axial and transverse tensile stresses, τ_S is the sliding shear stress in the fiber direction and τ_T is the transverse shear stress. Fiber bending resistance gives rise to a *couple stress*, or moment per unit area, m. The use of couple stresses to account for bending stiffness that would otherwise be lost in the development of material models has been employed before [for example, Biot, (1967)]. For a detailed discussion of the theory of couple stresses in continuum mechanics see, for example, Koiter (1964). Neglecting higher order terms, equilibrium of forces in the axial direction implies that the axial stress in the composite is constant and

$$\sigma_L \approx -\sigma^\infty. \tag{9}$$

Equilibrium of forces in the transverse direction gives

$$\frac{\partial \sigma_T}{\partial y} + \frac{\partial \tau_T}{\partial x} + \sigma_L\left(\frac{\partial \phi}{\partial x} + \frac{\partial \bar{\phi}}{\partial x}\right) \approx 0 \tag{10}$$

and equilibrium of moments gives

$$\frac{\partial m}{\partial x} = \tau_S - \tau_T. \tag{11}$$

When m is not constant, the stress tensor is not symmetric and $\tau_S \neq \tau_T$. On making

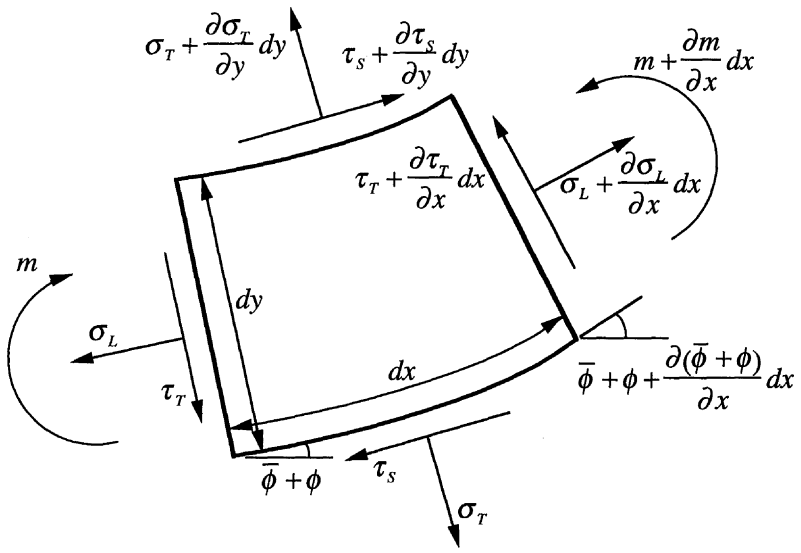

Fig. 3. Composite material element acted on by averaged stresses in the couple stress model.

use of the assumption of perfect correlation in the direction **c**, (9)–(11) are combined and integrated to give

$$\frac{\partial m}{\partial x}+\sigma^{\infty}(\bar{\phi}+\phi)=\tau_S+\sigma_T\tan\beta. \tag{12}$$

Constitutive relations

The couple stress m within the composite is due solely to the bending stiffness of the fibers. The fibers are assumed to be circular cylinders of diameter d and to deform elastically with Young's modulus E_f. From elastic beam theory the couple stress is related to the fiber curvature $d\phi/dx$ by

$$m=\frac{cE_fd^2}{16}\frac{d\phi}{dx}, \tag{13}$$

where c is the fiber volume concentration. If the elastic modulus of the fibers is much greater than that of the matrix then the quantity cE_f may be interpreted as an approximation to the elastic modulus of the composite in the fiber direction, E.

The composite is considered to behave as a compressible deformation theory solid with nonlinear strain hardening. The constitutive equations used are those proposed by Budiansky and Fleck (1993). Assume that the composite material is characterized by the quadratic yield condition

$$\left(\frac{\tau_S}{\tau_y}\right)^2+\left(\frac{\sigma_T}{\sigma_{Ty}}\right)^2=1, \tag{14}$$

where τ_y and σ_{Ty} are the plane strain yield stresses in simple shear in the fiber direction and in tension in the transverse tension, respectively. An equivalent shear stress,

$$\tau_e\equiv\sqrt{\tau_S^2+\sigma_T^2/R^2}, \tag{15}$$

is used as a plastic potential, with $R\equiv\sigma_{Ty}/\tau_y$ describing the eccentricity of the yield surface in (τ_S, σ_T) space. Provided the condition $R^2=E_T/G$ is satisfied, where E_T and G are the transverse and shear elastic moduli of the composite, then it can be shown from relations (8) and (14)–(15) that

$$\left.\begin{aligned}\gamma&=\frac{\tau_S}{G_S(\tau_e)}\\ \varepsilon_T&=\frac{\sigma_T}{R^2G_S(\tau_e)}\end{aligned}\right\}, \tag{16}$$

where $G_S(\tau_e)$ is the pure shear secant modulus. Budiansky and Fleck (1993) have shown that $R^2=E_T/G$ is a reasonable approximation for polymer matrix composites. An effective strain is defined by

$$\gamma_e \equiv \frac{\tau_e}{G_S(\tau_e)} \tag{17}$$

and it can be shown that

$$\left.\begin{aligned} \tau_S + \sigma_T \tan\beta &= \alpha\tau_e \\ \gamma = \phi &= \gamma_e/\alpha \end{aligned}\right\}, \tag{18}$$

where

$$\alpha \equiv \sqrt{1+R^2\tan^2\beta}. \tag{19}$$

The three-parameter Ramberg–Osgood strain hardening relation (5) is given in terms of the secant modulus by

$$\frac{G}{G_S(\tau_e)} = 1+\frac{3}{7}\left(\frac{\tau_e}{\tau_y}\right)^{n-1} \tag{20}$$

and will be used to describe the composite response throughout the remainder of this paper.

Equations (13) and (17)–(19) are used to rewrite (12) as a nonlinear second-order differential equation for $\phi(x)$. This equation can be given more concisely by defining the nondimensional quantities

$$\psi \equiv \frac{\phi}{\gamma_y^*}, \quad \bar{\psi} \equiv \frac{\bar{\phi}}{\gamma_y^*}, \quad \Lambda \equiv \frac{\sigma^\infty}{G^*}, \quad s \equiv \frac{\tau_e}{\tau_y}, \quad \xi \equiv \frac{4x}{d}\sqrt{\frac{G^*}{E}}, \tag{21}$$

where $\gamma_y = \tau_y/G$ has already been defined as the fiber shear yield strain and

$$\left.\begin{aligned} G^* &\equiv \alpha^2 G \\ \gamma_y^* &\equiv \gamma_y/\alpha \end{aligned}\right\}. \tag{22}$$

This leads to the nondimensional equation for the compressive response of the composite

$$\frac{d^2\psi}{d\xi^2} + \Lambda(\psi+\bar{\psi}) = s, \tag{23}$$

where s is related to ψ by the nondimensional form of the Ramberg–Osgood relation,

$$\psi = s[1+\tfrac{3}{7}|s|^{n-1}]. \tag{24}$$

In the limit $n \to \infty$, (24) describes an elastic–perfectly plastic response. To consider an elastic composite response let $s = \psi$ in (23). Equations (23) and (24) are used to solve for the collapse response of the composite for a given distribution of fiber misalignment $\bar{\psi} \equiv \bar{\phi}/\gamma_y^*$. Note that the dependence on the kink band angle β is contained within the nondimensionalization. To obtain results in dimensional form a value for β must be assumed. It can be seen from (8) and (16) that the composite undergoes proportional loading. Since proportional loading is maintained, the above deformation theory analysis provides the same results as a flow theory analysis and

is appropriate provided the effective stress $s(\xi)$ is monotonically increasing everywhere in the composite. The deformation and flow theories diverge when elastic unloading occurs.

Solution procedure

In the initial unloaded, stress-free state the composite has a misalignment distribution $\bar{\psi}(\xi)$. Under increasing remote load the composite deforms at each point along its length and, in principle, one can solve for $\psi(\xi)$ as a function of Λ. If a critical load for microbuckling exists, Λ goes through a maximum value Λ_c as deformation evolves; Λ_c is the critical microbuckling load and is obtained by solving for the load Λ as a function of some measure of the overall deformation which continues to increase as Λ goes through its maximum.

To proceed, let $\psi_1 \equiv \psi$, $\psi_2 \equiv \mathrm{d}\psi/\mathrm{d}\xi$ and $\psi_3 \equiv \Lambda$ (i.e. Λ is viewed as a "function" of ξ with zero spatial gradient). Decompose the second-order differential equation (23) into two coupled, first-order differential equations and write $\mathrm{d}\Lambda/\mathrm{d}\xi = 0$ to get

$$\left.\begin{aligned} \frac{\mathrm{d}\psi_1}{\mathrm{d}\xi} &= \psi_2 \\ \frac{\mathrm{d}\psi_2}{\mathrm{d}\xi} &= s(\psi_1) - \psi_3(\psi_1 + \bar{\psi}) \\ \frac{\mathrm{d}\psi_3}{\mathrm{d}\xi} &= 0 \end{aligned}\right\}, \tag{25}$$

where $s(\psi_1)$ is given by (24). By treating the load as a *dependent variable* in the system (25), it is explicitly solved once three boundary conditions have been specified. It is then possible to solve for the deformation response through any extrema in remote load. Let the ends of the composite be at $\xi = 0$ and $\xi = L$ and assume that zero moment is supported at the ends. Then, from (13),

$$\psi_2(0) = \psi_2(L) = 0. \tag{26}$$

The third condition required for a unique solution of the system of equations (25) is a prescribed value for the maximum fiber rotation ψ_m occurring anywhere along the length of the composite. The point along the composite where $\psi_1 = \psi_m$ is designated ξ_m, such that

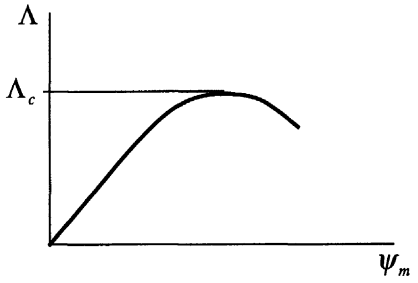

Fig. 4. Anticipated form of the solution for the couple stress model, showing the remote compressive stress Λ versus maximum fiber rotation ψ_m occurring anywhere along the length of the composite. The maximum sustainable stress Λ_c is the critical stress for microbuckling.

$$\psi_1(\xi_m) = \psi_m, \tag{27}$$

where $0 \leqslant \xi_m \leqslant L$. The anticipated composite response is shown in Fig. 4. This result is obtained by incrementally increasing ψ_m. At each increment the previous solution for ψ_1, ψ_2 and ψ_3 is used as the starting guess for the numerical algorithm and the initial guess for ξ_m is taken to be the value of ξ at which the maximum value of ψ_1 occurred in this previous step. For the first increment, the initial guess for ξ_m is taken to be the value of ξ at which the maximum value of $\bar{\psi}$ occurs. In practice it was found that ξ_m is nearly constant. A full discussion of the numerical algorithm is given in Appendix A. For each increment in ψ_m, it is verified that elastic unloading has not occurred anywhere along the composite. Should elastic unloading occur the predicted response would become sensitive to the assumed form of the plasticity relations: upon unloading the deformation theory solid gives a softer incremental response than that of flow theory. Whether deformation theory or flow theory is the more appropriate remains an open issue for epoxy matrix composites.

SINUSOIDAL WAVINESS

The kinking model of microbuckling (Budiansky and Fleck, 1993) neglects fiber waviness and provides an estimate for the critical load as a function of the initial fiber misalignment angle. It is unable to predict the effect of wavelength of waviness upon the collapse response. The couple stress model, as described above, is needed in order to determine the effect of the wavelength of initial fiber misalignment upon the collapse load. Assume a sinusoidal initial waviness of the form

$$\bar{\psi}(\xi) = \bar{\psi}_m \cos\left(\frac{2\pi\xi}{\lambda}\right), \tag{28}$$

where the amplitude $\bar{\psi}_m$ and the wavelength λ are independent parameters. By symmetry, a distribution $\psi(\xi)$ which is a solution to the differential equation (23) and the boundary conditions (26) for a composite length of one wavelength, $L = \lambda$, can be repeated to obtain a distribution $\psi(m\lambda + \xi) = \psi(\xi)$, where $m = 1,2,\ldots$, that satisfies (23) and (26) for any composite length L that is an integer multiple of the wavelength λ. The remote load Λ versus maximum fiber angle ψ_m will be the same. Therefore, equate the value of L in the boundary condition (26) with λ and consider the composite to be of infinite length. The remote load Λ versus maximum fiber angle ψ_m are shown in Fig. 5 for different values of the Ramberg–Osgood parameter n, as well as the elastic response. The amplitude and wavelength of the initial misalignment distribution in Fig. 5 are $\bar{\psi}_m = 5$ and $\lambda = 100$. Typical parameter values for a carbon fiber–epoxy matrix composite are $\alpha = 1.2$, $\gamma_y = 0.01$ and $E/G = 25$ (and $4\sqrt{G^*/E} \approx 1$) so that, in physical units, the initial misalignment angle in Fig. 5 has an amplitude and wavelength of 2.4° and 100 fiber diameters, respectively. These values are representative for carbon fiber–epoxy composites [see, for example, Budiansky and Fleck (1993)].

It is clear from Fig. 5 that the composite displays a maximum remote load Λ_c at a finite level of deformation and that subsequent deformation occurs at decreasing load. For moderate values of n, Λ_c decreases as n increases, but Λ_c increases again as $n \rightarrow$

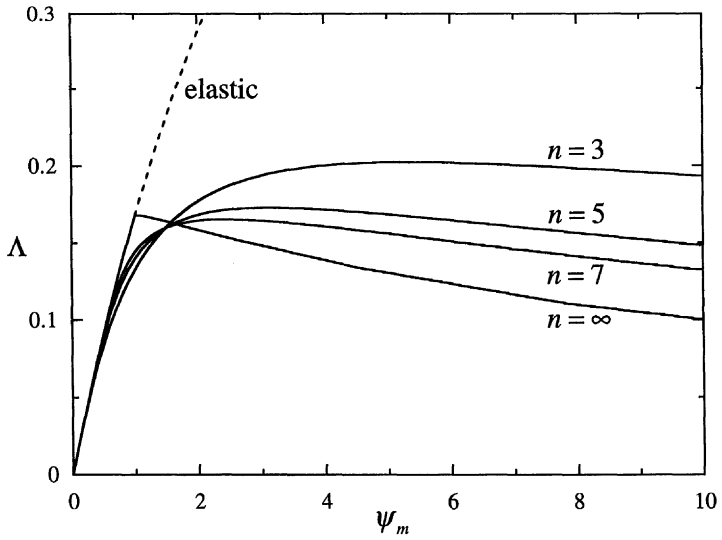

Fig. 5. Effect of the Ramberg–Osgood hardening parameter n upon the collapse response of load Λ versus maximum fiber angle ψ_m, for a sinusoidal initial fiber waviness, $\bar{\psi} = 5\cos(\pi\xi/50)$.

∞. The profile of fiber rotation, $(\bar{\psi}+\psi)$ versus ξ, is shown in Fig. 6 for $n = 5$ and for a range of loads up to the critical load Λ_c. It can be seen that plastic strain concentrates near the location of maximum initial misalignment, creating a kink band, as the load approaches the critical level $\Lambda/\Lambda_c \to 1$. $|\psi|$ is a maximum at fixed locations $\xi = k\lambda/2$, where k takes on all integer values. No elastic unloading occurs until *after* the critical load Λ_c has been obtained. Unloading does occur in regions outside the kink band post-maximum load. If the plastic response of the composite is closer to that of a flow theory solid than that of a deformation theory solid, then the post-maximum load response shown in Fig. 5 is only qualitatively correct, but the critical value of load Λ_c itself is accurate.

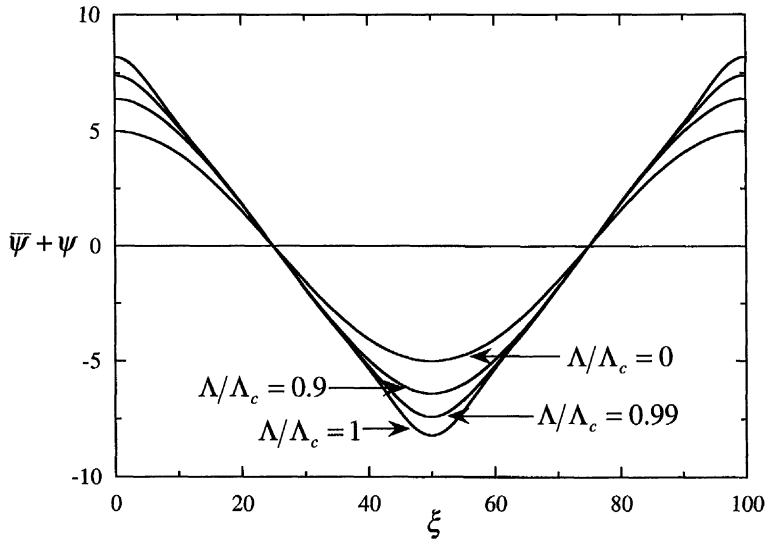

Fig. 6. The profile of fiber misalignment $(\bar{\psi}+\psi)$ under monotonically increasing remote stress. Λ_c is the critical stress for microbuckling. The initial fiber waviness is given by $\bar{\psi} = 5\cos(\pi\xi/50)$ and the Ramberg–Osgood hardening parameter is $n = 5$.

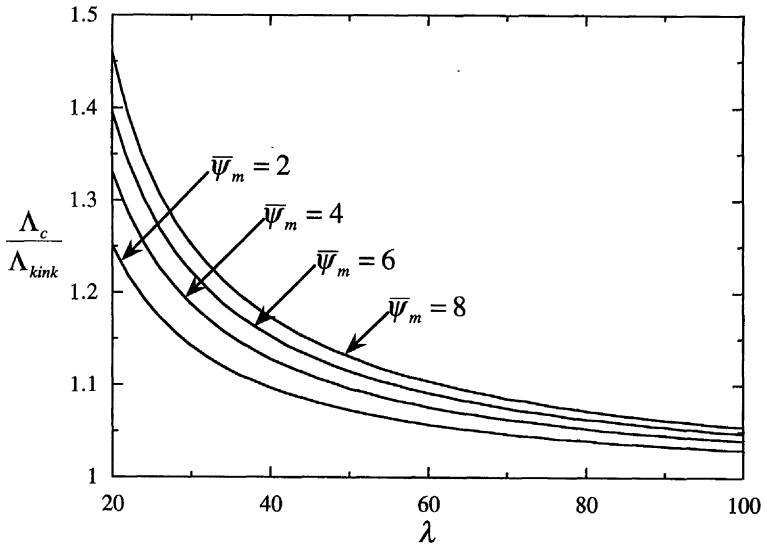

Fig. 7. The critical stress for microbuckling Λ_c, normalized by the kinking model solution Λ_{kink}, as a function of wavelength λ. The initial fiber waviness is $\bar{\psi} = \bar{\psi}_m \cos(2\pi\xi/\lambda)$ and the Ramberg–Osgood hardening parameter is $n = 5$.

A comparison can be made between the critical microbuckling load predicted by the *couple stress model* and the *kinking model* discussed in the introduction. In terms of the nondimensional quantities introduced in (21), the *kinking model* strength is given by rewriting (6) in the form

$$\Lambda_{\text{kink}} = \frac{1}{1 + n\left(\frac{3}{7}\right)^{1/n}\left(\frac{\bar{\psi}_m}{n-1}\right)^{(n-1)/n}}, \tag{29}$$

where the maximum value for the misalignment distribution $\bar{\psi}_m$ is assumed. The ratio of critical load predicted by the couple stress model to that of the kinking model, $\Lambda_c/\Lambda_{\text{kink}}$ is plotted in Fig. 7 against the wavelength of initial misalignment λ, for $\bar{\psi}_m = 2,4,6,8$ and $n = 5$. The critical load predicted by the couple stress model is higher for short wavelengths and asymptotes towards the kinking model prediction as the wavelength becomes infinite. Short wavelength imperfections are much less deleterious and the kinking model provides a lower, conservative bound for the compressive strength.

RANDOM WAVINESS

In engineering composites, fiber misalignment is stochastic rather than sinusoidal in nature. If one assumes that the fibers are perfectly correlated in the direction **c**, as previously defined in Fig. 2, and that the fiber misalignment distribution along the fiber direction is statistically independent of position, i.e. that it is a stationary function, then the random waviness can be characterized by its spectral density (Newland, 1984). The spectral density is a function which gives information about the mean square amplitude of a random signal associated with different frequencies

ω (or wavelengths). The total area under the spectral density curve is equal to the overall mean square value of the signal. Spectral density is defined as the Fourier transform of the autocorrelation function. It is assumed that the random fiber waviness of engineering composites can be characterized by the spectral density of the *fiber slope* $S(\omega)$, where fiber slope m is related to the fiber waviness angle $\bar{\phi}$ by $m \equiv \tan\bar{\phi}$.

No measurements of the spectral density for fiber waviness have been reported in the literature. Therefore, the approach adopted in the present study is to assume a simple form for the spectral density. Monte Carlo methods are used to generate an ensemble of fiber waviness profiles from the assumed spectral density. The collapse response for each realization of fiber shape is calculated and probability curves of collapse strength are obtained. Thus, the relationship between spectral density and the distribution of collapse strength is obtained. The problem is analogous to buckling of a beam on a nonlinear foundation with random initial imperfections, where the connection has been obtained between the spectral density of the imperfection distribution and the probability of buckling (Fraser and Budiansky, 1969). Monte Carlo methods have recently been used by Engelstad and Reddy (1994) in a study of variability in the properties of high-temperature metal matrix composites.

Monte Carlo simulation is a brute force technique for analyzing statistically the behavior of random systems. A large population of specimen representing a random system is generated, the response of each specimen to the desired stimuli is measured and appropriate statistical descriptions of the response of the *population* are determined. To implement the Monte Carlo method for the microbuckling problem, it is necessary to generate populations of random fiber misalignment distributions. For a given spectral density $S(\omega)$, individual realizations of fiber misalignment profile (in the form of fiber slope m) are created using an inverse fast Fourier transform (FFT) method (Cebon and Newland, 1984). Each realization will have zero mean fiber slope and the desired spectral density. For a detailed description of the method by which the realizations are constructed, see Appendix B.

The spectral density for fiber slope is taken to be a square wave, symmetric about the origin. The cut-off frequency of the square wave is ω_0 and the area under the spectral density curve from $\omega = -\omega_0$ to $\omega = \omega_0$ is $E[m^2]$, the mean square value of the fiber slope. A cut-off frequency in the spectral density implies that there is a minimum fiber wavelength, which is a reasonable assumption for fibers of finite bending stiffness. Other forms of the spectral density function were also tried: the results were found to be relatively insensitive to the shape of the function, but sensitive to the cut-off frequency and to the mean square value. Since $S(\omega)$ is the spectral density associated with $m(x)$, the resulting realizations are in the form of fiber slope m as a function of position along the composite, x. It is necessary to specify values for γ_y^* and $4\sqrt{G^*/E}$ in order to relate information about the initial fiber waviness derived from $S(\omega)$ to the normalized parameter $\bar{\psi}(\xi)$ needed for (25)–(27). The values $\gamma_y^* \approx 0.008$ and $4\sqrt{G^*/E} \approx 1$ are assumed, as these are typical for a carbon fiber–epoxy matrix composite. It is instructive to consider the probability density for maximum initial misalignment $p(\bar{\psi}_m)$ derived through Monte Carlo simulation, as shown in Fig. 8 for $E[m^2] = 4 \times 10^{-4}$, $\omega_0 = 0.25$ and composite length $L = 400$. $\omega_0 = 0.25$ corresponds to a minimum wavelength of about 25 fiber diameters. The magnitude of

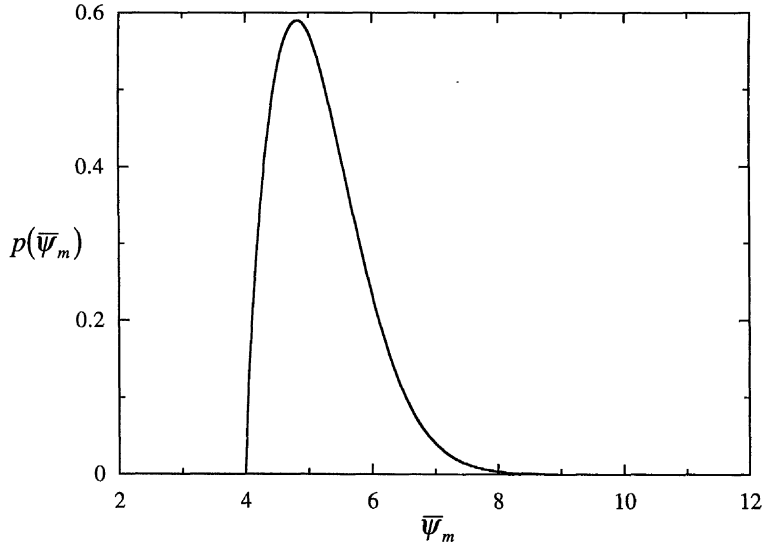

Fig. 8. Probability density function for the maximum initial fiber misalignment $p(\bar{\psi}_m)$ from the Monte Carlo simulation. 500 realizations, $\omega_0 = 0.25$, $E[m^2] = 4 \times 10^{-4}$, $L = 400$.

fiber waviness depicted in Fig. 8 is reasonably representative of the observed fiber waviness in carbon fiber epoxy systems, as reported for example by Yurgartis (1987) and Jelf and Fleck (1992). (An initial misalignment angle of $\bar{\psi} = 5$ corresponds to $\bar{\phi} = 2.3°$.)

Each Monte Carlo realization of the fiber shape is analyzed, using the couple stress formulation, to determine its critical stress for microbuckling. Figures 9 and 10 show typical results for a representative realization with $\omega_0 = 0.25$, $E[m^2] = 4 \times 10^{-4}$, composite length $L = 400$ and Ramberg–Osgood parameter $n = 5$. The fiber misalignment profile, $(\bar{\psi} + \psi)$ versus ξ, is shown in Fig. 9 for the unloaded and critically loaded composite. It

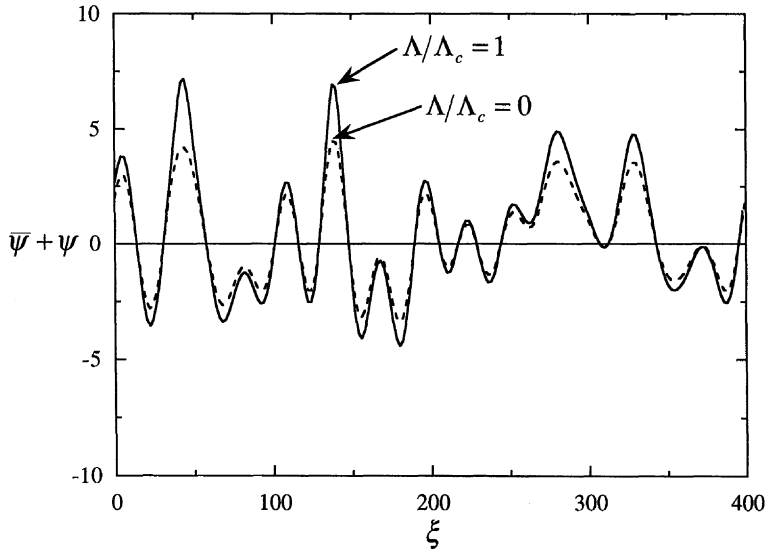

Fig. 9. The fiber misalignment profile, $(\bar{\psi} + \psi$ versus $\xi)$, for an unloaded composite ($\Lambda = 0$) and critically loaded composite ($\Lambda = \Lambda_0$) with random initial fiber waviness. $\omega_0 = 0.25$, $E[m^2] = 4 \times 10^{-4}$, $L = 400$ and $n = 5$.

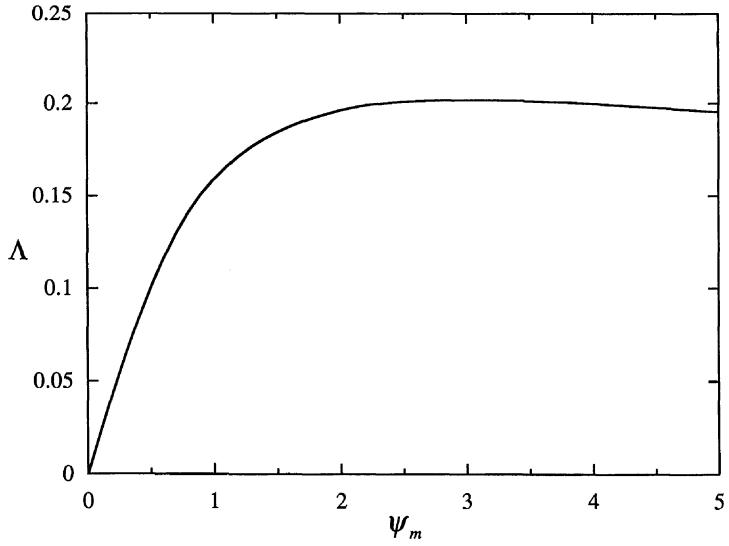

Fig. 10. Remote load Λ versus maximum fiber angle ψ_m for a composite with random initial fiber waviness. $\omega_0 = 0.25$, $E[m^2] = 4 \times 10^{-4}$, $L = 400$ and $n = 5$.

can be seen that plastic deformation concentrates at the locations of maximum initial misalignment. Figure 10 shows the load Λ versus maximum fiber rotation occurring in the composite ψ_m. It is clear from Fig. 10 that the load goes through a maximum. No elastic unloading occurs anywhere in the composite prior to the critical load being attained.

After a suitably large population of realizations has been generated and analyzed, the cumulative probability function for microbuckling stress $P(\Lambda_c)$ is computed. This is shown in Fig. 11 for the above parameters and 500 realizations. The probability curve is well matched by the Weibull curve

$$P(\Lambda_c) = 1 - \exp\left[-\left(\frac{\Lambda_c - \Lambda_u}{\Lambda_0}\right)^m\right], \tag{30}$$

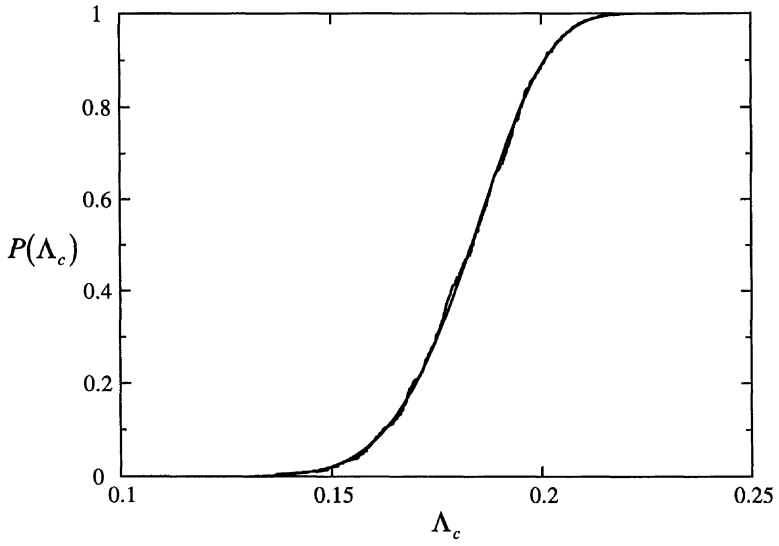

Fig. 11. Cumulative probability function for microbuckling stress $p(\Lambda_c)$ from the Monte Carlo simulation with 500 realizations ($\omega_0 = 0.25$, $E[m^2] = 4 \times 10^{-4}$, $L = 400$, $n = 5$). Also shown in a Weibull curve, with parameters obtained by a least squares fit.

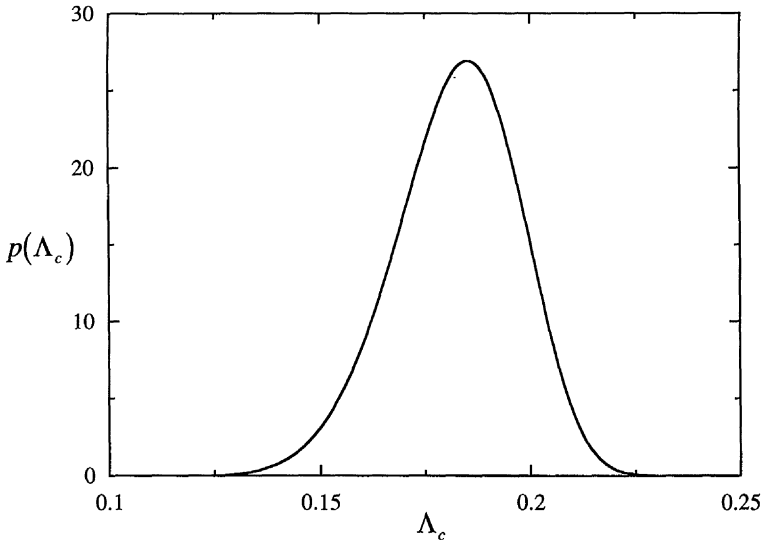

Fig. 12. Probability density function for microbuckling stress $p(\Lambda_c)$ from the Monte Carlo simulation with 500 realizations ($\omega_0 = 0.25$, $E[m^2] = 4 \times 10^{-4}$, $L = 400$, $n = 5$).

where the fitting parameters $\Lambda_u = 0.1129$, $\Lambda_0 = 7.536 \times 10^{-2}$ and $m = 5.408$ have been determined through a least squares algorithm. Jelf and Fleck (1992) have determined the Weibull modulus m for carbon fiber reinforced PEEK: they find m to be 6.1, which is in reasonable agreement with the value for $m = 5.4$ found here.

The empirical function (30) can be differentiated to give the probability density function $p(\Lambda_c)$ shown in Fig. 12. (The probability density function from the ensemble of Monte Carlo simulations shows a large degree of scatter associated with the numerical differentiation involved and is omitted for the sake of clarity.) The Monte Carlo results are adequately fitted by (30), but it is noted that small changes in Λ_u and Λ_0 lead to large changes in m, while the deviation from the Monte Carlo simulation remains very small. Consequently, an attempt to relate the fitting parameters to spectral density input parameters for the Monte Carlo simulation is difficult and has not been attempted. The remaining results of this paper will be presented as probability density curves without further reference to actual Weibull parameter values. In order to compare the predictions of the couple stress model and the kinking model the maximum value of initial fiber misalignment angle $\bar{\psi}_m$ in each Monte Carlo realization is substituted into (29) for the kinking strength Λ_{kink}. The predicted strength from the couple stress model Λ_c for the same fiber shape is also determined; in this manner, the probability density function $p(\Lambda_c/\Lambda_{kink})$ is computed for the population of realizations. A typical result is shown in Fig. 13; in this instance the couple stress model gives predictions which are 10–15% stronger than that of the kinking model.

The effect of composite length L upon the probability density function of failure $p(\Lambda_c)$ is shown in Fig. 14, for $\omega_0 = 0.25$, $E[m^2] = 4 \times 10^{-4}$ and $n = 5$. As the composite length L increases, the probability density curve becomes narrower and shifts towards lower values of critical load. The probability of occurrence of a high amplitude imperfection with long associated wavelength increases with increasing length of composite sample L and one would, therefore, expect lower critical stresses. An attempt can be made to predict the results for different composite lengths based on

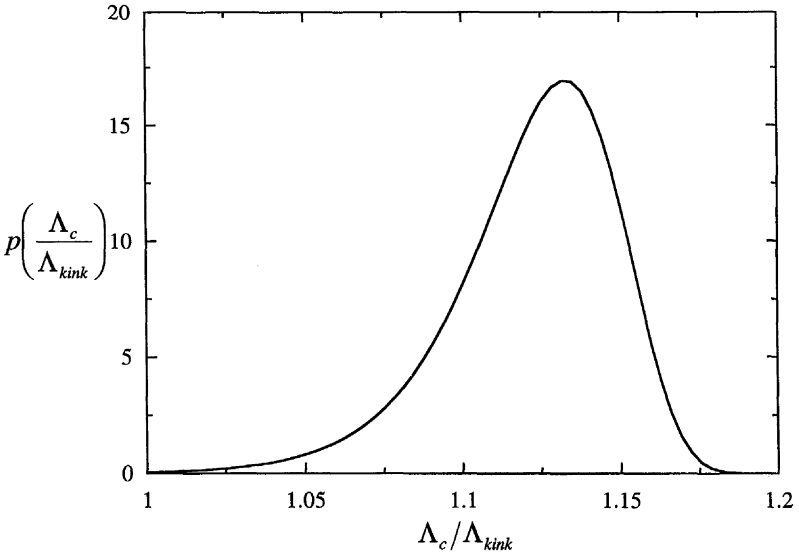

Fig. 13. Probability density function for the microbuckling stress predicted by the couple stress model, normalized by the kinking model results, $p(\Lambda_c/\Lambda_{kink})$ from the Monte Carlo simulation with 500 realizations ($160_0 = 0.25$, $E[m^2] = 4 \times 10^{-4}$, $L = 400$, $n = 500$).

Weibull "weakest link" statistics, so that upon differentiation of (30) with respect to Λ_c, one finds

$$p(\Lambda_c) = \frac{mL}{\Lambda_0 L_0}\left(\frac{\Lambda_c - \Lambda_u}{\Lambda_0}\right)^{m-1} \exp\left[-\left(\frac{\Lambda_c - \Lambda_u}{\Lambda_0}\right)^m \frac{L}{L_0}\right], \tag{31}$$

where L_0 is the reference length and Λ_u, Λ_0 and m are the fitting parameters for the Monte Carlo simulation at that length. The predictions of (31) are shown in Fig. 14, where the reference length has been taken to be $L_0 = 400$, along with the results of

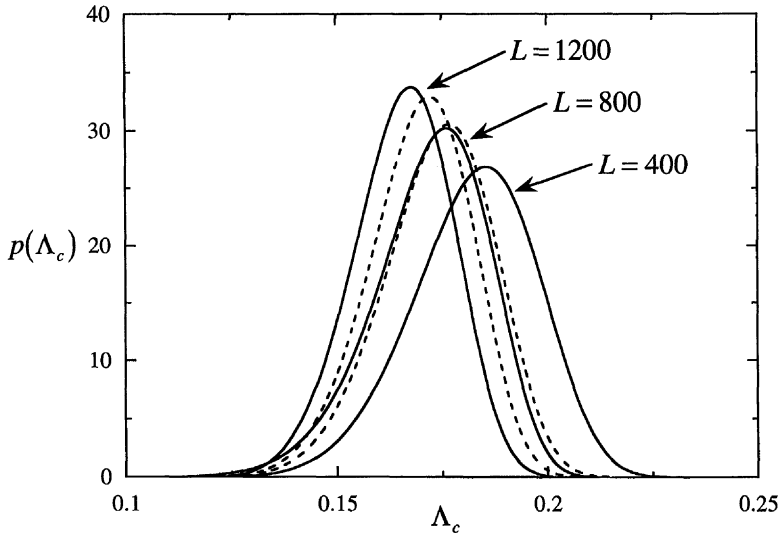

Fig. 14. Effect of composite length upon the probability density function for microbuckling $p(\Lambda_c)$ ($\omega_0 = 0.25$, $E[m^2] = 4 \times 10^{-4}$, $n = 5$). The Monte Carlo simulation predictions are shown as solid lines and the Weibull "weakest link" predictions are shown as dashed lines.

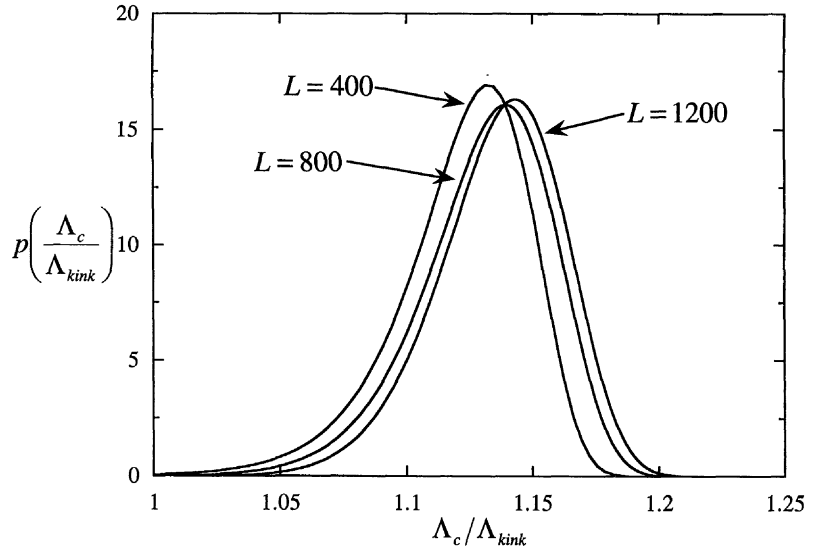

Fig. 15. Effect of composite length on the probability density function for the critical microbuckling stress, normalized by the kinking model strength, $p(\Lambda_c/\Lambda_{kink})$. $\omega_0 = 0.25$, $E[m^2] = 4 \times 10^{-4}$ and $n = 5$.

the Monte Carlo simulations. The Weibull predictions successfully give the correct trend for $p(\Lambda_0)$, but do not accurately reproduce the results of the Monte Carlo simulations. The poor agreement is associated with the particular functional form assumed by Weibull for the stress dependence on the probability of failure: it is fully expected that the one-dimensional Monte Carlo simulations give rise to weakest link behavior by the following argument.

Weakest link behavior is simply a corollary of the feature that each segment of the composite is statistically independent of its neighbors. Consider two random samples of wavy composite of length L_1 and L_2. Then, weakest link theory dictates that, for a fixed value of applied stress, the probability of survival of a sample of length $(L_1 + L_2)$ equals the probability of survival of the sample of length L_1 times the probability of survival of the sample of length L_2. Provided the samples are of sufficient individual length to make irrelevant the particular end condition assumed, the Monte Carlo simulations give rise to weakest link behavior. Further, as the length becomes infinite the limiting form of the probability density function for microbuckling becomes a Dirac delta function at a fixed level of stress (the microbuckling stress for an infinite composite is unique for a given spectral density). According to the Weibull equation (31), this limiting stress is Λ_u. It is expected that the limiting stress of the Monte Carlo simulation is zero at infinite composite length $L \to \infty$. Figure 15 shows the probability density for the normalized microbuckling stress, $p(\Lambda_c/\Lambda_{kink})$, for the same composite lengths as in Fig. 14. Recall from the analysis of sinusoidal waviness that, for large wavelengths λ, Λ_c/Λ_{kink} decreases only slowly with increasing λ. This is consistent with the observation in Fig. 15 that $p(\Lambda_c/\Lambda_{kink})$ is approximately independent of composite length. The increased probability of a high amplitude, long wavelength imperfection which is accordant with an increase in composite length has only a small effect on $p(\Lambda_c/\Lambda_{kink})$.

The effect of the particular choice of cut-off frequency ω_0 upon the probability density function for the critical microbuckling stress is shown in Figs 16 and 17, for

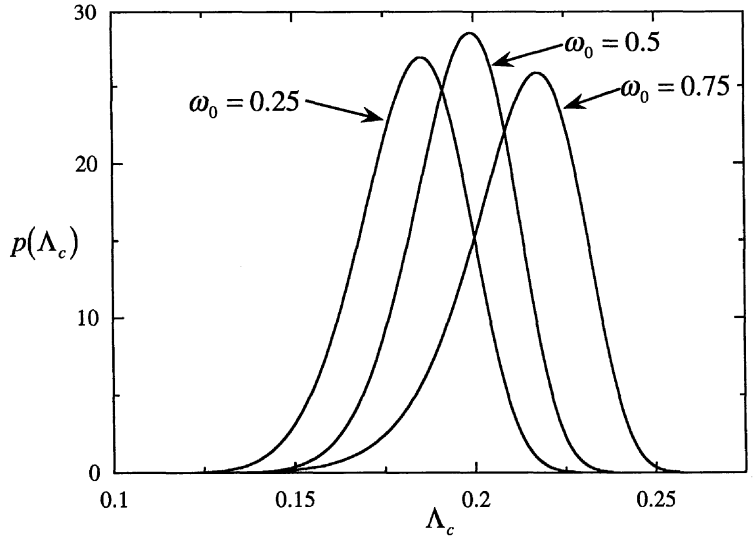

Fig. 16. Effect of cut-off frequency ω_0 on the probability density function for the critical microbuckling stress $p(\Lambda_c)$. $E[m^2] = 4 \times 10^{-4}$, $L = 400$ and $n = 5$.

a fixed $E[m^2] = 4 \times 10^{-4}$, $L = 400$ and $n = 5$. It is seen from Fig. 16 that as ω_0 increases, the probability density $p(\Lambda_c)$ shifts towards higher values of stress while its width remains nearly constant. A consideration of the power spectral density reveals that as the cut-off frequency increases, while the area under the function curve remains constant, the relative area associated with short frequencies (i.e. long wavelengths) decreases. Consequently, the probability of occurrence of deleterious high amplitude imperfections associated with long wavelengths decreases and higher strengths are expected. The effect is more pronounced for $p(\Lambda_c/\Lambda_{kink})$, as shown in Fig. 17. As ω_0 increases, the fiber shape contains a higher proportion of high frequency, short wavelength waviness; the associated increase in the maximum value of fiber mis-

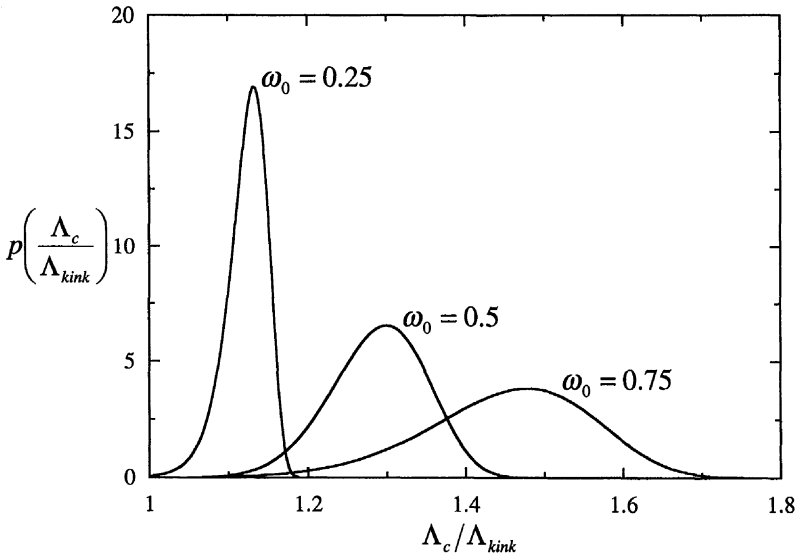

Fig. 17. Effect of cut-off frequency ω_0 on the probability density function for the critical microbuckling stress, normalized by the kinking model strength, $p(\Lambda_c/\Lambda_{kink})$. $E[m^2] = 4 \times 10^{-4}$, $L = 400$, $n = 5$.

alignment angle $\bar{\psi}$ produces lower predicted kink strengths. Thus, $p(\Lambda_c/\Lambda_{kink})$ is shifted toward higher values of Λ_c/Λ_{kink} and the width of the probability density curve is markedly increased. It is concluded that for large values of cut-off frequency (say, $\omega_0 > 0.5$) the kinking model ceases to give an accurate prediction of microbuckling stress for random fiber waviness.

DISCUSSION

By including the fiber bending stiffness in the analysis of fiber microbuckling, it is seen that the critical microbuckling stress depends upon both the amplitude and the wavelength of initial fiber waviness. If the wavelength is short, the fiber curvature associated with an amplitude is large and the fiber bending stiffness provides a significant contribution to the compressive strength of the composite. As the wavelength increases, the fiber curvature associated with an amplitude decreases and, consequently, so does the strengthening due to fiber bending stiffness. The kinking model analysis, which neglects the fiber bending stiffness, is equivalent to the couple stress model when the initial imperfection wavelength is infinite. For all wavelengths, the kinking model gives a conservative estimate of failure load.

The couple stress model is used to predict the compressive response of composites with random fiber waviness. It is seen that fiber rotation is concentrated around the regions of maximum initial misalignment; at maximum load, deformation concentrates into microbuckles, or kink bands, and the composite fails. Probability density functions for the critical compressive stress for microbuckling are predicted for given spectral densities of initial fiber misalignment using a Monte Carlo simulation method. The results show that the kinking model analysis, while giving a lower bound, can significantly underestimate the compressive strength for certain spectral densities of misalignment.

The results of this paper illustrate the need for studies of the spectral density of fiber misalignment in real composite materials. The authors are aware of measurements of the probability density of fiber misalignment (e.g. Yurgartis, 1987), but these studies have not included any information on the fiber misalignment wavelength. Once such spectral densities are determined, the analysis presented here may be used to predict the probability of compressive failure.

The current study may be viewed as a prototype for the effect of imperfection magnitude and wavelength upon shear localization in other solids. The central feature is that failure is governed not only by the magnitude of the imperfection (in this case the magnitude of the fiber misalignment angle) but also the length scale of the imperfection *relative* to the material length scale (in this case, set by fiber bending stiffness). The discrete Fourier transform proves to be a useful tool for the generation of an ensemble of structural realizations from an assumed spectral density function. This approach shows promise in providing a rigorous micromechanical basis for empirical statistical parameters such as the Weibull theory of strength.

ACKNOWLEDGEMENTS

The authors wish to thank Professor B. Budiansky for several helpful discussions during the early stages of the study. Financial support from the ONR grant 0014-91-J-1916 is gratefully

acknowledged. Additional financial support is acknowledged from the Procurement Executive of the Ministry of Defense.

REFERENCES

Argon, A. S. (1972) Fracture of composites. *Treatise of Materials Science and Technology*, Vol. 1. Academic Press, New York.

Biot, M. A. (1967) Rheological stability with couple stresses and its application to geological folding. *Proc. R. Soc. A* **298,** 402–423.

Budiansky, B. (1983) Micromechanics. *Comput. Struct.* **16,** 3–12.

Budiansky, B. and Fleck, N. A. (1993) Compressive failure of fiber composites. *J. Mech. Phys. Solids* **41,** 183–211.

Cebon, D. and Newland, D. E. (1984) The artificial generation of road surface topography by the inverse FFT method. *Proc. 8th IAVSD Symp. on the Dynamics of Vehicles on Roads and on Tracks*, MIT, Cambridge, MA, 15–19 August, 1983. Swets and Zeitlinger, Amsterdam.

Christensen, R. M. (1993) On compressive failure of fibrous composites. *Comp. Engng* **3,** 1111–1118.

Daniel, I. M., Hsiao, H.-M., Wooh, S. C. and Vittoser, J. (1993) Processing and compressive behavior of thick composites. *Proc. 1st ASME/ASCE/SES Joint Mechanics Conf.*, Charlottesville, VA 6–9 June, 1993. *ASME AMD-Vol.* 162, *Mechanics of Thick Composites* (Ed. Y. D. S. Rajapakse), pp. 107–126.

Engelstad, S. P. and Reddy, J. N. (1994) Probabilistic methods for the analysis of metal-matrix composites. *Comp. Sci. Technol.* **50,** 91–107.

Evans, A. G. and Adler, W. F. (1978) Kinking as a mode of structural degradation in carbon fiber composites. *Acta Metall.* **26,** 725–738.

Fleck, N. A., Deng, L. and Budiansky, B. (1993) Prediction of kink width in fiber composites. *J. Appl. Mech.* (submitted).

Fraser, W. B. and Budiansky, B. (1969) The buckling of a column with random initial deflections. *J. Appl. Mech.* **36,** 232–240.

Huang, Y. H. and Wang, S. S. (1989) Compressive fatigue damage and associated property degradation of aluminium-matrix composite. *Proc. 4th Jap.–U.S. Conf. on Composite Materials*, Washington., DC 27–29 June, 1988, pp. 606–632. Technomic, Westport, CT.

Hull, D. (1981) *An Introduction to Composite Materials.* Cambridge University Press, Cambridge.

Jelf, P. M. (1993) Compressive failure of aligned fiber composites. Ph.D. thesis, Cambridge University Engineering Department, Cambridge.

Jelf, P. M. and Fleck, N. A. (1992) Compressive failure mechanisms in unidirectional composites. *J. Comp. Mater.* **26,** 2706–2726.

Koiter, W. T. (1964) Couple stresses in the theory of elasticity, I and II. *Proc. Ned. Akad. Wet. B* **67,** 17–44.

Lagoudas, D. S., Tadjbakhsh, I. and Fares, N. (1991) A new approach to microbuckling of fibrous composites. *J. Appl. Mech.* **58,** 473–479.

Newland, D. E. (1984). *An Introduction to Random Vibrations and Spectral Analysis*, 2nd edn. Wiley, New York.

Press, W. H., Flannery, B. P., Teukolsky, S. A. and Vetterling, W. T. (1986) *Numerical Recipes.* Cambridge University Press, Cambridge.

Rosen, B. W. (1965) Mechanics of composite strengthening. *Fiber Composite Materials*, pp. 37–75. American Society of Metals Seminar, Metals Park, OH.

Sadowsky, M. A., Pu, S. L. and Hussain, M. A. (1967) Buckling of microfibers. *J. Appl. Mech.* **34,** 1011–1016.

Schapery, R. A. (1993) Compressive strength and failure time based on local buckling in viscoelastic composites. *Appl. Mech. Rev.* **46** (11), Part 2, S221–S228.

Schapery, R. A. (1994) Prediction of compressive strength and kink bands in composites using

a work potential. University of Texas Report No. SSM-94-1, presented at *A Symposium on the Occasion of the 60th Birthday of Wolfgang G. Knauss*, California Institute of Technology, 1–2 February, 1994 *Int. J. Solids Struct.* (To be published).

Schulte, K. and Minoshima, K. (1991) Mechanisms of fracture and failure in metal matrix composites. *12th Risø Int. Symp on Materials Science: Metal Matrix Composites Processing, Microstructure, and Properties* (ed. N. Hansen *et al.*), pp. 123–147.

Slaughter, W. S. and Fleck, N. A. (1993a) Compressive fatigue of fiber composites. *J. Mech. Phys. Solids* **41,** 1265–1284.

Slaughter, W. S. and Fleck, N. A. (1993b) Viscoelastic microbuckling of fiber composites. *J. Appl. Mech.* **60,** 802–806.

Slaughter, W. S., Fleck, N. A. and Budiansky, B. (1993) Compressive failure of fiber composites; the roles of multi-axial loading and creep. *J. Engng Mater. Technol.* **115,** 308–313.

Steif, P. S. (1987) An exact two-dimensional approach to fiber micro-buckling. *Int. J. Solids Struct.* **23,** 1235–1246.

Yurgartis, S. W. (1987) Measurement of small angle fiber misalignments in continuous fiber composites. *Comp. Sci. and Technol.* **30,** 279–293.

APPENDIX A: NUMERICAL ALGORITHM FOR TWO-POINT BOUNDARY VALUE PROBLEMS WITH AN INTERNAL CONSTRAINT

The numerical algorithm used to solve the system of first order differential equations (25), subject to the boundary conditions (26) and the "internal" condition (27), is a modification of the relaxation method for two-point boundary value problems (Press *et al.*, 1986). The strategy is to solve iteratively for the deformed fiber shape and the remote load as the maximum value of fiber rotation along its length is increased in incremental steps. Let the composite length be meshed over M equally spaced points, so that

$$\xi_k \equiv \frac{(k-1)}{(M-1)} L, \quad (k = 1, 2, \ldots, M), \tag{A1}$$

and define the following mesh point quantities:

$$\left.\begin{aligned} &\psi_{1,k} \equiv \psi_1(\xi_k), \quad \psi_{2,k} \equiv \psi_2(\xi_k), \quad \psi_{3,k} \equiv \psi_3(\xi_k) \\ &\boldsymbol{\psi}_k = [\psi_{1,k} \quad \psi_{2,k} \quad \psi_{3,k}]^{\mathrm{T}} \end{aligned}\right\}. \tag{A2}$$

In (A2) and following, bold notation is used to define column matrix quantities. The mesh points defined by (A1) are uniformly distributed along the composite in this analysis, but this is not a requirement of the algorithm. The system (25) is then expressed as the system of finite difference equations ($k = 2, 3, \ldots, M$),

$$\left.\begin{aligned} 0 = E_{1,k} &= \psi_{1,k} - \psi_{1,k-1} - \Delta\xi_k \tilde{\psi}_{2,k} \\ 0 = E_{2,k} &= \psi_{2,k} - \psi_{2,k-1} - \Delta\xi_k \{s(\tilde{\psi}_{1,k}) - \tilde{\psi}_{3,k}[\tilde{\psi}_{1,k} + \bar{\psi}(\tilde{\xi}_k)]\} \\ 0 = E_{3,k} &= \psi_{3,k} - \psi_{3,k-1} \\ \mathbf{0} = \mathbf{E}_k(\boldsymbol{\psi}_k, \boldsymbol{\psi}_{k-1}) &= [E_{1,k} \quad E_{2,k} \quad E_{3,k}]^{\mathrm{T}} \end{aligned}\right\}, \tag{A3}$$

where $\Delta\xi_k \equiv \xi_k - \xi_{k-1}$, $\tilde{\xi}_k \equiv \frac{1}{2}(\xi_k + \xi_{k-1})$ and $\tilde{\boldsymbol{\psi}}_k \equiv \frac{1}{2}(\boldsymbol{\psi}_k + \boldsymbol{\psi}_{k-1})$. There are $3M$ unknowns $\boldsymbol{\psi}_k$ for which (A3) provides $3(M-1)$ equations. The remaining three equations are provided by the conditions (26)–(27),

$$\left.\begin{aligned} 0 &= B_1 = \psi_{2,k} \\ 0 &= B_2 = \psi_{1,I} - \psi_m, \\ 0 &= B_3 = \psi_{2,M} \end{aligned}\right\} \tag{A4}$$

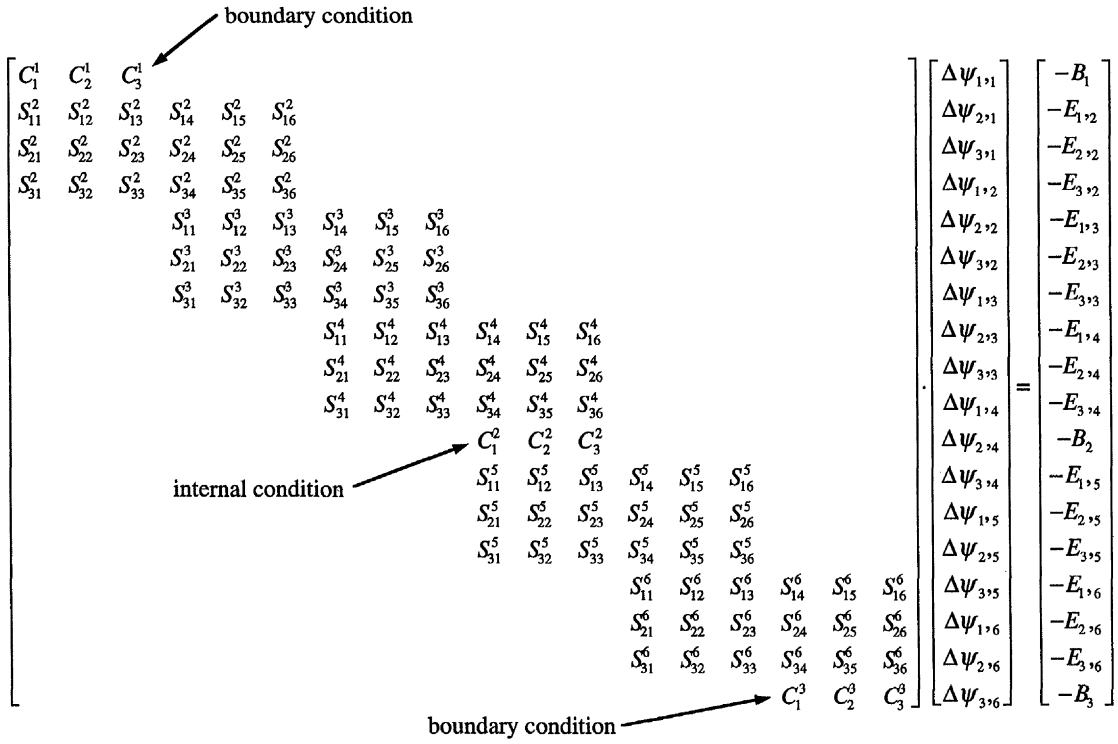

Fig. A1. Form of the banded coefficient matrix arising in the numerical analysis of two-point boundary value problems with internal conditions.

where ψ_m is the prescribed maximum value of fiber rotation occurring anywhere along the composite and I is the mesh point at which ψ_m occurs. How I is determined will be discussed shortly.

The system of coupled, homogeneous equations (A3) and (A4) is solved using the Newton–Raphson method. An initial guess is provided for $\boldsymbol{\psi}_k$ and the corrections $\Delta\boldsymbol{\psi}_k$ are determined such that $\boldsymbol{\psi}_k + \Delta\boldsymbol{\psi}_k$ is an improved approximation for the solution. Taking the first-order Taylor expansion of $\mathbf{E}_k$ with respect to $\Delta\boldsymbol{\psi}_k$ and noting that the improved approximation should satisfy (A3), gives

$$\mathbf{0} = \mathbf{E}_k(\boldsymbol{\psi}_k + \Delta\boldsymbol{\psi}_k, \boldsymbol{\psi}_{k-1} + \Delta\boldsymbol{\psi}_{k-1}) \approx \mathbf{E}_k(\boldsymbol{\psi}_k, \boldsymbol{\psi}_{k-1}) + \sum_{j=1}^{3} \frac{\partial \mathbf{E}_k}{\partial \psi_{j,k-1}} \Delta\psi_{j,k-1} + \sum_{j=1}^{3} \frac{\partial \mathbf{E}_k}{\partial \psi_{j,k}} \Delta\psi_{j,k}. \quad \text{(A5)}$$

Thus, $3(M-1)$ linear equations for the corrections can be written as

$$\sum_{j=1}^{3} S_{ij}^{k} \Delta\psi_{j,k-1} + \sum_{j=4}^{6} S_{ij}^{k} \Delta\psi_{j-3,k} = -E_{i,k}, \quad i = 1,2,3, \quad k = 2,3,\ldots,M, \quad \text{(A6)}$$

where

$$S_{ij}^{k} = \frac{\partial E_{i,k}}{\partial \psi_{j,k-1}}, \quad S_{i(j+3)}^{k} = \frac{\partial E_{i,k}}{\partial \psi_{j,k}}, \quad j = 1,2,3. \quad \text{(A7)}$$

Similarly, the boundary and internal conditions, $B_1(\psi_1)$, $B_2(\psi_1)$ and $B_3(\psi_M)$, can be expressed in terms of the corrections as

$$\sum_{j=1}^{3} C_j^i \Delta\psi_{j,k} = -B_i, \quad C_j^i = \frac{\partial B_i}{\partial \psi_{j,k}}, \quad \text{(A8)}$$

where the node numbers i and k have the relative values: if $i = 1$ then $k = 1$; if $i = 2$ then

$k = I$; and if $i = 3$ then $k = M$. The derivatives in (A7) and (A8) are obtained analytically from (A3) and (A4). This makes $3M$ linear equations for $3M$ unknown corrections $\Delta\psi_k$. If carefully constructed, the coefficient matrix is banded with a band width of 9. An example of this construction, for $M = 6$ and $I = 4$ is given in Fig. A1. A common algorithm for the solution of banded linear systems allows the problem to be solved efficiently.

I is taken to be the mesh point where the maximum value of the initial guess for $\psi_{1,k}$ occurs. The above procedure is repeated, updating ψ_k (and I, if necessary) each time, until the corrections $\Delta\psi_k$ are sufficiently small. For the first iteration, ψ_k is provided by the solution from the previous increment of ψ_m in the couple stress analysis. This iterative scheme is nested within a mesh refinement iteration. The number of mesh points M is increased until the predicted value of remote load $\Lambda = \psi_3$ has converged to within 0.1%.

APPENDIX B: GENERATING RANDOM DISTRIBUTIONS BASED ON A GIVEN SPECTRAL DENSITY

Consider first a distribution f(x), sampled discretely over the interval $x = (0,L)$. Let $f_k \equiv f(x_k)$, where $x_k = k\Delta$, $k = 0,1,\ldots,N-1$ and $\Delta = L/N$. The discrete Fourier transform (DFT) of f_k is (Newland, 1984)

$$F_k = \frac{1}{N}\sum_{r=0}^{N-1} f_r \exp\left(-i\frac{2\pi kr}{N}\right), \quad k = 0,1,\ldots,N-1. \tag{B1}$$

If ω_0 is the maximum frequency component present in f(x), then it is required that $N > \omega_0 L/\pi$ in order to avoid aliasing (an accuracy eroding artifact of the implicit assumption that the sampled distribution is periodic). An important property of F_k is that $F_{N+k} = F_k$ and $F_{-k} = F_k^*$, where F_k^* is the complex conjugate of F_k, so that

$$\left.\begin{aligned} |F_{-k}| &= |F_k| \\ |F_{N-k}| &= |F_k| \end{aligned}\right\}. \tag{B2}$$

$S(\omega)$, the spectral density of f(x), is defined as the Fourier transform of its autocorrelation function. It can be shown, however, that in discrete form, with $S_k \equiv S(\omega_k)$ and $\omega_k \equiv 2\pi k/N\Delta$, the spectral density is related to the DFT by

$$S_k \approx \frac{N\Delta}{2\pi} F_k^* F_k = \frac{N\Delta}{2\pi}|F_k|^2. \tag{B3}$$

It follows from (B2) that

$$\left.\begin{aligned} S_{-k} &= S_k \\ S_{N-k} &= S_k \end{aligned}\right\}, \tag{B4}$$

i.e. the specification (B3) for the spectral density is symmetric about the origin and is uniquely defined only on the interval $k = (0, N/2)$.

Given a spectral density function $S(\omega)$, how does one generate random realizations of the discrete distribution $f_k = f(kL/N)$ of length L and refinement $\Delta = L/N$? Following the procedure outlined by Cebon and Newland (1984):

(1) Identify a cut-off frequency ω_0 above which $S(\omega)$ is zero (or approximately zero). Choose an *even* integer N appropriate for the desired refinement and satisfying $N > \omega_0 L/\pi$.

(2) Sample the spectral density and enforce the constraint (B4) to obtain S_k:

$$\left.\begin{aligned} S_k &= S\left(\frac{2\pi k}{N\Delta}\right), \quad k = 0,1,\ldots,\frac{N}{2} \\ S_{N-k} &= S_k, \quad k = 1,2,\ldots,\frac{N}{2}-1 \end{aligned}\right\}. \tag{B5}$$

(3) From (B3), the magnitude of the DFT of the distribution f(x) is

$$|F_k| = \sqrt{\frac{2\pi}{N\Delta} S_k} \tag{B6}$$

and it is required that $F_{N+k} = F_k$ and $F_{N-k} = F_k^*$; the phase angle of F_k must be periodic in the interval $k = (0,N)$ and antisymmetric with respect to $k = N/2$. The phase is otherwise taken to be random with uniform probability distribution between 0 and 2π. The DFT is thus given by

$$F_k = \left(\sqrt{\frac{2\pi}{N\Delta} S_k}\right) e^{i\theta_k}, \tag{B7}$$

where

$$\left.\begin{aligned} &\theta_k \text{ is random}, \quad k = 1,2,\ldots,\frac{N}{2}-1 \\ &\theta_{N-k} = -\theta_k, \quad k = 1,2,\ldots,\frac{N}{2}-1 \\ &\theta_k = 0, \quad k = 0 \quad \text{and} \quad \frac{N}{2} \end{aligned}\right\}. \tag{B8}$$

(4) The random discrete distribution is given by the inverse DFT of (B7),

$$f_k = \sum_{r=0}^{N-1} F_r \exp\left(i\frac{2\pi kr}{N}\right), \quad k = 0,1,\ldots,N-1. \tag{B9}$$

The discrete transform (B9) can be efficiently evaluated by using the fast Fourier transform (FFT) algorithm. The resulting random realizations will be real valued and have zero mean and the specified spectral density. They will also be periodic over the interval $k = (0,N)$, i.e. $f_0 = f_N$, but it is assumed that this will not affect the results of the Monte Carlo simulation.